Synthesis of mesoporous $LaPO_4$ nanostructures with controllable morphologies†

Zhanli Chai,[ab] Li Gao,[a] Cheng Wang,*[a] Hongjie Zhang,[a] Rongkun Zheng,[c] Paul A. Webley[b] and Huanting Wang*[b]

Received (in Victoria, Australia) 4th February 2009, Accepted 28th May 2009
First published as an Advance Article on the web 2nd July 2009
DOI: 10.1039/b902381j

Lanthanum phosphate ($LaPO_4$) nanostructures with different morphologies were prepared by a facile solution–precipitation process. The effect of different reaction conditions on the morphology of nanostructures was studied. When the molar ratio of La^{3+} : H_3PO_4 was around 1 : 2, 1 : 20, 1 : 100, and 1 : 200, four different morphologies, such as near-spherical, snowflake-like, star-shaped, lens-like nanostructures and short nanorods, were obtained, respectively. Meanwhile, similar shapes developed when the molar ratio of H_3PO_4 to ionic surfactants, such as SDS and CTAB, was varied. In addition, Eu^{3+} doped and Ce^{3+}/Tb^{3+} co-doped $LaPO_4$ nanostructures showed morphology evolution similar to undoped $LaPO_4$ nanostructures. The optical properties of these doped $LaPO_4$ were also characterized.

Introduction

The properties of nanomaterials depend not only on their chemical composition, structures, and phases but also on their shapes, sizes and size distributions.[1–3] Over the past few years, the synthesis of building blocks of low-dimensional nanostructured inorganic materials has been the focus of research;[4,5] currently there is growing interest in the construction of functionalised, ordered superstructures and complex architectures.[6–8] Self-assembly is one of the most effective approaches to produce complex nanostructures with or without the assistance of surfactants and copolymers.[9–11] This self-assembly process is usually driven by interactions between individual building blocks such as electrostatic interactions, van der Waals interactions or hydrogen bonding. For example, a monolayer of alkyl chain molecules can be attached to the surface of monodispersed nanocrystals and be viewed as capping agents. The interactions among the alkyl chain molecules can prevent aggregation and precipitation of nanocrystals and help to stabilize the final nanocrystal array.[12] Besides these alkyl chain molecules, organic surfactants with long or branched alkyl chains such as trioctylphosphine oxide (TOPO) or tributyl phosphate (TBP) have also been widely applied for the same purpose.[9]

Lanthanide orthophosphates ($LnPO_4$) and their nanocrystals offer a variety of potential applications, such as for phosphors, sensors, proton conductors, ceramic materials, catalysts, and heat-resistant materials.[13–15] In contrast to nano-scale semiconductors[16] and noble metals,[17] whose optical properties are dependant on their dimensional sizes and morphologies, the electronic transitions for rare earth based luminescent materials are localized within their 4f orbitals, which are shielded by outer orbitals.[18] Therefore no quantum confinement for such luminescent materials would be expected regardless of their particle sizes. On the other hand, with a decrease in particle size or a variation of shape, the symmetry of luminescent rare earth metal sites could be altered as a result of increased surface atomic ratio or phase change. This potentially offers an alternative approach to tuning the properties of Lanthanide orthophosphates. In addition, the synthesis of rare earth based luminescent materials with controlled morphologies and a narrow size distribution is important for the fabrication of devices. The synthesis of Ln^{3+} doped $LaPO_4$ nanostructures (Ln = Eu, Tb, Tb/Ce, *etc.*) with controlled compositions, dimensional sizes and morphologies have attracted much research interest recently.[19–22] Many synthetic methods including hydrothermal synthesis,[23,24] high-boiling-solvent technique,[12,13,25] sol–gel,[26] precipitation,[27] emulsion,[28] and microwave-assisted synthesis[29] have been developed for the synthesis of rare earth phosphate nanostructures. Various $LnPO_4$ nanostructures, such as one dimensional nanowires, nanorods and monodispersed nanoparticles have been prepared using the above-mentioned techniques.

Here we present a facile moderate-temperature solution–precipitation approach for synthesizing mesoporous $LaPO_4$ nanostructures and their Eu^{3+} doped ($LaPO_4$:Eu) and Ce^{3+}/Tb^{3+} co-doped ($LaPO_4$:Ce,Tb) derivatives. $LaPO_4$ nanostructures with different morphologies, such as spherical, snowflake-like, star-shaped, lens-like nanostructures and nanorods were synthesized when the molar ratio of La^{3+} : H_3PO_4 was changed. Meanwhile, the same shape evolution was observed by adjusting the molar ratio of H_3PO_4 : additional ionic surfactants, such as sodium dodecyl sulfate (SDS) and cetyl trimethylammonium bromide (CTAB). In addition, those doped $LaPO_4$ ($LaPO_4$:Eu, $LaPO_4$:Ce,Tb)

[a] *State Key Laboratory of Rare Earth Resource Utilization, Changchun Institute of Applied Chemistry, Chinese Academy of Sciences, Changchun 130022, P. R. China. E-mail: cwang@ciac.jl.cn*
[b] *Department of Chemical Engineering, Monash University, Clayton, Victoria 3800, Australia. E-mail: huanting.wang@eng.monash.edu.au*
[c] *Australian Key Center for Microscopy and Microanalysis, The University of Sydney, Sydney, Australia*

† Electronic supplementary information (ESI) available: Synthetic details; additional SEM images and spectra. See DOI: 10.1039/b902381j

nanostructures also had a similar shape evolution as the molar ratio of La^{3+} : H_3PO_4 was varied.

Results and discussion

Snowflake-like $LaPO_4$ nanostructures

Fig. 1a shows the XRD pattern of $LaPO_4$ nanostructures obtained in a typical synthesis (the molar ratio of La^{3+} : H_3PO_4 = 1 : 20). All diffraction peaks can be indexed to a pure monoclinic phase (JCPDS No. 35-0531), which exhibits a monazite structure with space group $P2_1/n$. From Fig. 1b, it can be seen that uniform snowflake-like nanostructures with a dimensional size of around 300 nm were obtained. The thickness of such snowflake-like nanostructures is about 150–200 nm. TEM images (Fig. 1c) show that the snowflake-like nanostructures consist of irregular nanoparticles, and thus they are polycrystalline in nature as further confirmed by the electron diffraction (ED) pattern (inset of Fig. 1c). The HRTEM results (Fig. 1d) reveal that these irregular nanoparticles have different growth habits, evidenced by various interplanar spacings such as 0.29, 0.31, and 0.33 nm, which correspond to the *d* spacings of the (012), (210), and (200) planes of monazite $LaPO_4$, respectively. These nanoparticles are about 5–8 nm in size and assemble into snowflake-like nanostructures *via* oriented attachment.

When the reaction time was increased from 10.0 min to 3.0 h at 150 °C, snowflake-like $LaPO_4$ nanostructures remained almost unchanged (Fig. S1 in the ESI†), which suggests fast growth and subsequent oriented attachment of the as-prepared nanoparticles. However, the reaction temperature does have some effect on the morphology of the products. As shown in Fig. S2†, star-shaped nanostructures with more distinct horns were prepared as the reaction temperature was increased.

We found that $LaPO_4$ nanostructures with different shapes (Fig. 2) could be obtained by changing the molar ratio of La^{3+} : H_3PO_4 (*i.e.*, changing the volume of H_3PO_4–EG). As shown in Fig. 2a, uneven near-spherical nanostructures with a diameter of 100–300 nm were obtained when the molar ratio of La^{3+} : H_3PO_4 was around 1 : 2 (0.1 ml of H_3PO_4–EG). As the molar ratio of La^{3+} : H_3PO_4 was increased to 1 : 20 (1.0 ml of H_3PO_4–EG), the uniform snowflake-like nanostructures shown in Fig. 1 were produced. When a molar ratio of 1 : 100 (5.0 ml of H_3PO_4–EG) was used, lens-shaped particles were dominant, and coexisted with star-shaped particles including hexagonal (Fig. 2b1), pentagonal (Fig. 2b2), and quadrangular (Fig. 2b3) pods. By further increasing the molar ratio of La^{3+} : H_3PO_4 to 1 : 200 (10.0 ml of H_3PO_4–EG), short nanorods with lengths of 400 nm and widths of 200 nm were synthesized (Fig. 2c). All these nanostructures were assembled from $LaPO_4$ nanoparticles and were polycrystalline in nature as indicated by TEM and ED results. In addition, the crystallinity of $LaPO_4$ nanostructures could be improved by increasing the molar ratio of La^{3+} : H_3PO_4 since the dispersive rings in their corresponding ED patterns gradually changed to dots from Fig. 2a to Fig. 2c. This observation was consistent with the XRD results (Fig. S3†). Further SEM images of nanostructures prepared using other molar ratios of La^{3+} : H_3PO_4 are also provided in Fig. S4 for comparison.†

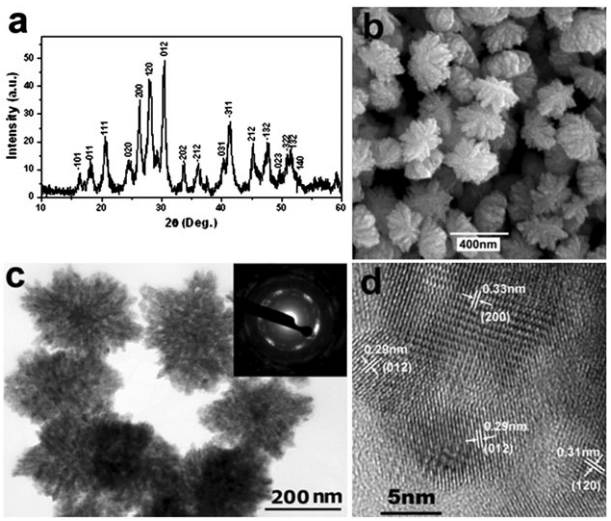

Fig. 1 The XRD (a), SEM (b), TEM (c), HRTEM (d) and electron diffraction pattern (inset of c) of $LaPO_4$ nanostructures obtained in a typical synthesis (molar ratio of La^{3+} : H_3PO_4 = 1 : 20).

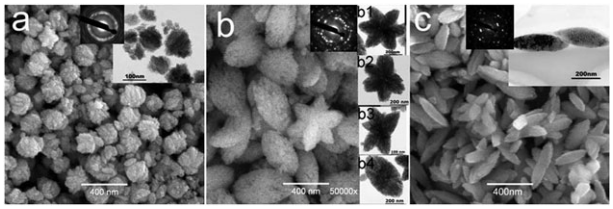

Fig. 2 SEM images and TEM insets of $LaPO_4$ nanostructures obtained in a typical synthesis with different volumes of H_3PO_4–EG. The different molar ratios of La^{3+} : H_3PO_4 are (a) 1 : 2 (b) 1 : 100 (c) 1 : 200. The insets beside the TEM images are the electron diffraction patterns.

Another important factor in determining the morphology and size of nanostructures was the use of organic additives. Without any organic additive, uniform nanoparticles with diameters of tens of nanometres were obtained (Fig. 3a). However, upon introduction of nonpolar organic additives, such as 1.0 ml TOPO, snowflake-like $LaPO_4$ nanostructures were produced (Fig. 3b). When the amount of TOPO was increased to 5.0 ml, snowflake-like nanostructures assembled from small nanoparticles were formed (Fig. 3c). If TOPO was used to replace all the EG (*i.e.*, 10.0 ml), very small nanoparticles with a diameter of less than 10 nm were obtained as shown in Fig. 3d. Besides TOPO, three other typical surfactants, *e.g.* non-ionic poly(vinyl pyrrolidone) (PVP), anionic SDS and cationic CTAB, were also used as organic additives in order to investigate their influence on the formation of $LaPO_4$ nanostructures. In a typical synthesis (the molar ratio of La^{3+} : H_3PO_4 = 1 : 20), the amounts of all reactants were fixed while the amount of surfactant was adjusted. Two molar ratios of surfactant : H_3PO_4 (1 : 10, and 1 : 100) were studied. As shown in Fig. 4a, snowflake-like $LaPO_4$ nanostructures were synthesized when the molar ratio of PVP : H_3PO_4 was around 1 : 10. However, lower molar ratio (1 : 100) of PVP : H_3PO_4 had no influence on the morphology

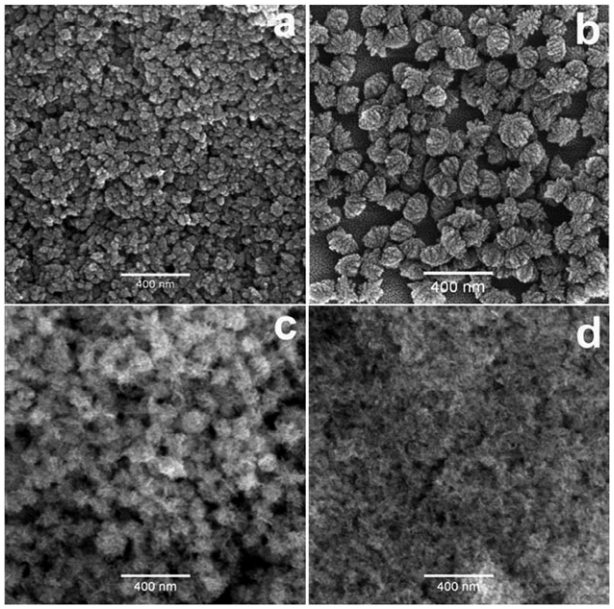

Fig. 3 SEM images of the $LaPO_4$ nanostructures obtained in a typical synthesis with the reactants of 0.35 mmol $La(NO_3)_3$ and 1.0 ml H_3PO_4–EG added to different solvents (a) 10.0 ml EG; (b) 1.0 ml TOPO and 9.0 ml EG; (c) 5.0 ml TOPO and 5.0 ml EG; (d) 10.0 ml TOPO.

of the final products (Fig. 4b). In the case of anionic SDS, near-spherical nanostructures were produced when the molar ratio of SDS : H_3PO_4 was about 1 : 10 (Fig. 4c). If the molar ratio of SDS : H_3PO_4 was lowered to 1 : 100, snowflake-like $LaPO_4$ nanostructures were obtained (Fig. 4d). For cationic CTAB, some branched nanorods were produced (Fig. 4e) when the molar ratio of CTAB : H_3PO_4 was 1 : 10. By reducing the molar ratio of CTAB : H_3PO_4 to 1 : 100, snowflake-like $LaPO_4$ nanostructures were synthesized as shown in Fig. 4f.

These four $LaPO_4$ nanostructures with different morphologies were analyzed by nitrogen sorption, and their nitrogen adsorption–desorption isotherms and pore size distributions are shown in Fig. 5. All samples exhibit a type IV adsorption–desorption isotherm with H1-type hysteresis, indicating they are mesoporous; such mesoporous structures are expected to arise from the self-assembly of nanoparticles. The samples a–d shown in Fig. 5, obtained from typical syntheses with different molar ratios of La^{3+} : H_3PO_4 (1 : 2, 1 : 20, 1 : 100, 1 : 200), have BET surface areas of 228, 156, 85, 36 $m^3\ g^{-1}$ and pore volumes of 0.75, 0.30, 0.31, 0.29 $cm^3\ g^{-1}$, respectively. It is noted that the spherical $LaPO_4$ sample exhibits a much greater surface area (228 $m^3\ g^{-1}$) and pore volume (0.75 $cm^3\ g^{-1}$) than the three others, and may find potential applications in catalysis and hydrogen storage.[14] The Barrett–Joyner–Halenda (BJH) pore-size distribution curves shown in the inset of Fig. 5 indicate that the pore sizes of these samples increase from a to d, and they are in the range of ~5, 5–10, 5–15 and 25–45 nm, respectively. This may be related to the crystallinity of the samples. As the crystallinity increases from a to d, the sizes of their building blocks (nanoparticles) increase, leading to greater packing pore sizes and lower pore volumes.

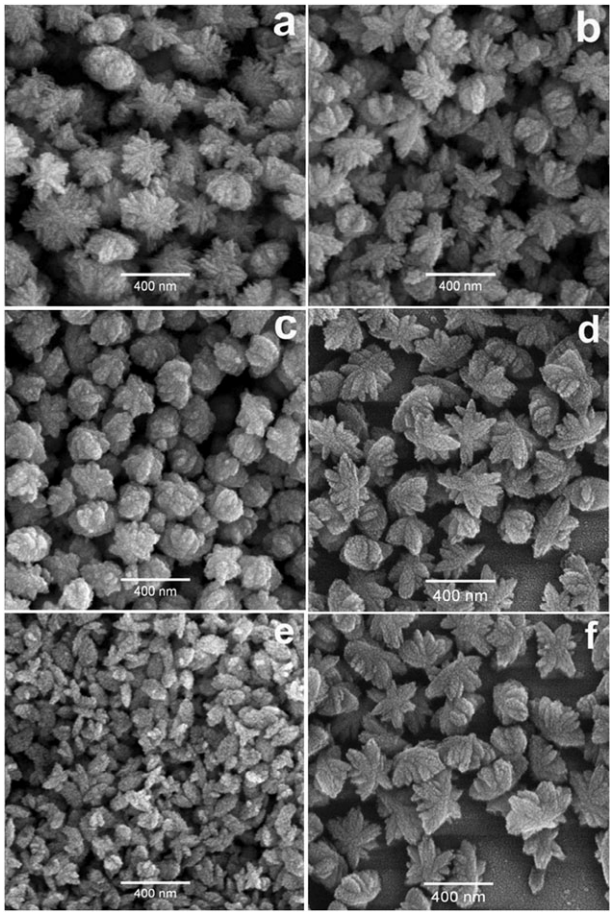

Fig. 4 SEM images of the $LaPO_4$ nanostructures obtained in a typical synthesis with different molar ratios of additional surfactants to H_3PO_4. (a) PVP : H_3PO_4 = 1 : 10 (0.7 mmol PVP); (b) PVP : H_3PO_4 = 1 : 100 (0.07 mmol PVP); (c) SDS : H_3PO_4 = 1 : 10 (0.7 mmol SDS); (d) SDS : H_3PO_4 = 1 : 100 (0.07 mmol SDS); (e) CTAB : H_3PO_4 = 1 : 10 (0.7 mmol CTAB); (f) CTAB : H_3PO_4 = 1 : 100 (0.07 mmol CTAB).

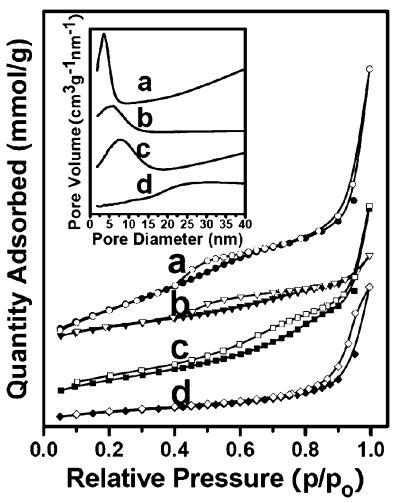

Fig. 5 N_2 adsorption–desorption isotherms and corresponding pore size distribution curves (inset) for as-synthesized $LaPO_4$ nanostructures in typical synthesis with different molar ratios of La^{3+} : H_3PO_4 of (a) 1 : 2 (b) 1 : 20 (c) 1 : 100 (d) 1 : 200.

Formation process of $LaPO_4$ nanostructures

$LaPO_4$ has a monazite structure and each lanthanide atom is coordinated by nine neighbouring oxygen atoms, which form a polyhedron of pentagonal interpenetrating tetrahedra. The nine-coordinate lanthanide atoms combine apically with distorted tetrahedral PO_4^{3-} groups to form chains along the *c* axis (or [001]) direction,[30] which induces the intrinsic anisotropic growth of $LaPO_4$. Organic additives, such as TOPO, are present in the final product as confirmed by FT-IR spectroscopy (Fig. S5†). They may be absorbed onto different crystalline facets *via* covalent bonding or electrostatic interactions, and then alter their surface energy. In addition, the absorbed TOPO might drag $LaPO_4$ nanoparticles out of EG solution, which then aggregate into sub-micrometre particles *via* oriented attachment (Fig. 3b/c). When TOPO is used as solvent without addition of EG, $LaPO_4$ monomers capped with TOPO would dissolve in TOPO and form small nanoparticles when the monomers reach supersaturation (Fig. 3d). Therefore, the presence of TOPO (<50%) that is immiscible with EG might be the key factor for the self-assembly of nanoparticles. The formation of our mesoporous nanostructured $LaPO_4$ is schematically depicted in Fig. 6. Firstly, the La–TOPO solution is added to EG. The mixture is heated to 80 °C in order to remove the cyclohexane from the La–TOPO extractive solution (Fig. 6a). After H_3PO_4–EG solution is added (Fig. 6b), the mixture is magnetically stirred for 30 min to ensure complete mixing of the reactants. Then uniform $LaPO_4$ nanocrystals are obtained when the solution mixture is heated to higher temperatures (Fig. 6c). The as prepared $LaPO_4$ nanocrystals self-assemble into different structures such as snowflake-like particles (Fig. 6d).

In our experiment, the synthesis reaction for formation of the $LaPO_4$ phase can be simplified as

$$La^{3+} + H_3PO_4 \rightarrow LaPO_4 + 3H^+ \quad (1)$$

As the volume of H_3PO_4–EG is increased, reaction (1) proceeds in the forward direction, and much more H^+ is released. When the volume of H_3PO_4–EG remains unchanged, the quantity of H^+ can be altered by addition of an ionic surfactant, such as SDS or CTAB. The introduction of anionic SDS consumes some H^+; whereas cationic CTAB quite easily combines with PO_4^{3-}, which produces more free H^+. As shown in Fig. 4c–f, mophology evolution occurs by decreasing the quantity of SDS or increasing the amount of CTAB, which is similar to the situation that occurs when the volume of H_3PO_4–EG is increased (Fig. 2). But the change of the amount of non-ionic PVP has nearly no effect on the morphology of $LaPO_4$ nanostructures, as revealed in Fig. 4a–b. All shapes of $LaPO_4$ nanostructures evolve when the amount of H^+ is varied. Therefore, the free H^+ is presumably the decisive factor for the morphology evolution.

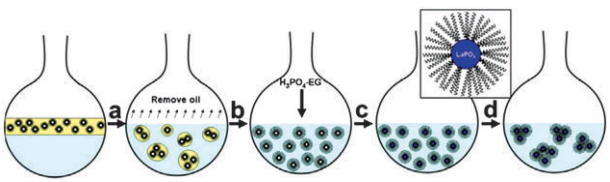

Fig. 6 Process scheme for the synthesis of $LaPO_4$ nanostructures using La–TOPO and H_3PO_4–EG as reactants. (a) evaporation of cyclohexane in the La–TOPO extractive solution; (b) addition of H_3PO_4–EG to the solution mixture; (c) formation of $LaPO_4$ nanocrystals at elevated temperatures; (d) self-assembly of the nanocrystals into nanostructures. Inset is a single $LaPO_4$ nanocrystal bonded to TOPO.

Eu^{3+} doped and Ce^{3+}/Tb^{3+} co-doped $LaPO_4$ nanostructures and their optical properties

Due to the empty 4f shell of La^{3+} and the lack of an f–f transition, $LaPO_4$ has been widely used as a host lattice to produce doped multicomponent lanthanide orthophosphate phosphors. In this study, our established synthetic methodology was extended to the synthesis of 5% Eu^{3+} doped and Ce^{3+}/Tb^{3+} (45%/15%) co-doped $LaPO_4$ nanostructures (their preparation procedures are described in the ESI†). The low dopant concentration is due to fluorescence quenching (or concentration quenching) where a molecule quenches its own fluorescence at high concentration. The reason for selecting Eu^{3+} as doping ion is that it retains the same symmetry site in the nanoparticle that it has in bulk powder. Ce^{3+}/Tb^{3+} co-doping has been applied in a commercialized phosphor with high efficiency. In both cases, XRD results (Fig. S6†) indicate that the doped products are monoclinic phase, and their diffraction peaks show small shifts as compared with undoped $LaPO_4$; EDX results confirm that Eu^{3+} and Ce^{3+}/Tb^{3+} ions were doped into the $LaPO_4$ nanostructures. This demonstrates the feasibility of our synthetic protocol. Meanwhile, the doped nanostructures show similar morphological evolutions to the undoped $LaPO_4$ nanostructures (Fig. 7 and Fig. S7†). Fig. 8 shows the room temperature excitation and emission spectra of 5% Eu^{3+} doped $LaPO_4$ nanostructures with different molar ratios of $La^{3+}:H_3PO_4$.

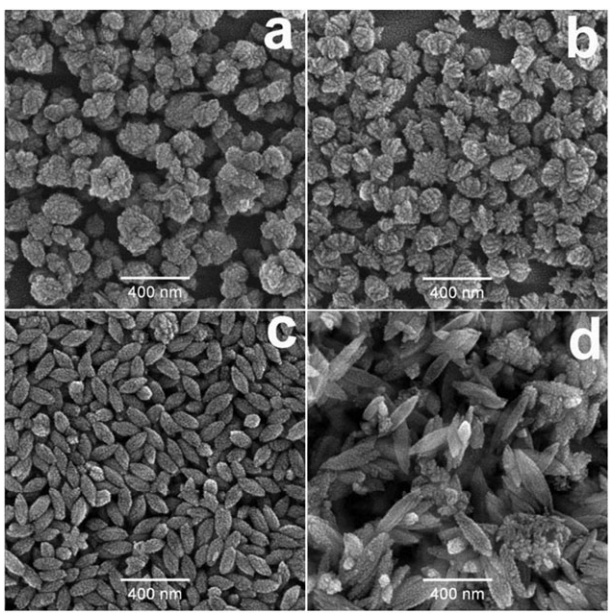

Fig. 7 SEM images of $LaPO_4$:Eu nanostructures synthesized in a typical synthesis with different molar ratio of $La^{3+}:H_3PO_4$ (a) 1 : 2 (b) 1 : 20 (c) 1 : 100 (d) 1 : 200.

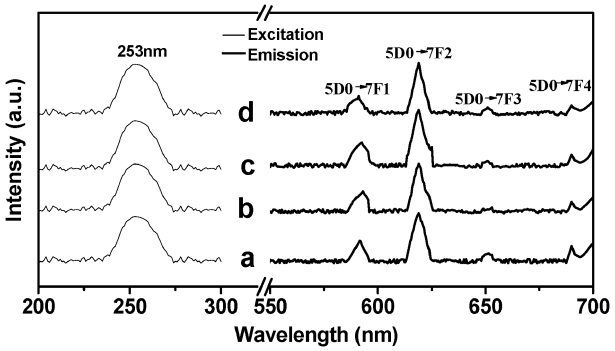

Fig. 8 Room temperature excitation and emission spectra of $LaPO_4$:Eu nanostructures synthesized in a typical synthesis with different molar ratio of $La^{3+}:H_3PO_4$ (a) 1 : 2 (b) 1 : 20 (c) 1 : 100 (d) 1 : 200 (λ_{ex} = 396 nm).

The strongest peak is the electric-dipole transition corresponding to $^5D_0$–$^7F_4$, which agrees with the low symmetry site of Eu^{3+} in the monoclinic structure. The absence of splitting of ^7F_J states in the spectra might preclude the contribution from a Eu^{3+} f–f transition within metal sites of nanoparticles. In the case of $LaPO_4$:Ce,Tb, the excitation spectrum (Fig. S8†) consists of four broad peaks with maxima at 221, 245, 260, and 272 nm (strongest), which correspond to the transitions from the ground state $^2F_{5/2}$ of Ce^{3+} to the different components of the excited Ce^{3+} 5d states when split by the crystal field. The emission lines are associated with the Tb^{3+} transitions from its $^5D_4$ level to ^7F_J levels. Although the crystallinity of $LaPO_4$:Eu and $LaPO_4$:Ce,Tb nanostructures can be improved and the morphologies are tunable with increasing molar ratio of $La^{3+}:H_3PO_4$, all four samples show similar luminescent spectra. This can be explained by the fact that all products with different morphologies are constructed from similar primary small nanoparticles, have fairly large specific surface area and are capped with organic additives.

Conclusions

We have described a simple solution–precipitation approach for the preparation of complex $LaPO_4$ nanostructures *via* oriented-attachment of small nanoparticles. The surfactants were crucial for guiding the self-attachment of nanoparticles. Nanostructures with different shapes, including spherical ones, snowflake-like ones, star-shaped ones and short nanorods, were produced when the molar ratio of $La^{3+}:H_3PO_4$ or additional ionic surfactants : H_3PO_4 was adjusted. The similarity between these two different reaction conditions was the variation of H^+ concentration, which was proven to be crucial for the morphology evolution of $LaPO_4$ nanostructures. The $LaPO_4$:Eu and $LaPO_4$:Ce,Tb nanostructures all showed a similar shape evolution to the undoped $LaPO_4$ nanostructures. Although their excitation and emission spectra were quite similar and showed no significant difference from their bulk materials, these nanostructures, with controlled morphologies and narrow size distributions, may show advantages for device fabrication. The morphology-controllable synthesis of mesoporous rare earth phosphate nanostructures presented in this paper has several merits including simplicity, good reproducibility and low cost, and thus contributes to the development of novel syntheses of inorganic mesoporous nanostructures.

Experimental

Typically, 1.0 ml of La–TOPO (0.35 mol l^{-1}, its preparation procedure is described in the ESI†) and 1.0 ml of H_3PO_4–EG (7.0 mol l^{-1}, its preparation procedure is described in the ESI†) were added to 10.0 ml of pure EG solvent (or 10.0 ml of EG solution containing 0.7 mmol of surfactant M (M = PVP, CTAB, SDS)) in a three-necked flask equipped with a condenser at room temperature. The resulting slurry was heated to 80 °C and put under vacuum for 30 min to remove water and low boiling point solvents, producing a transparent solution. Afterwards, the resulting mixture was kept at 150 °C for 24 h, leading to a slightly white turbid solution. The resultant mixture was centrifugally separated and the products were collected. The solid products were washed with ethanol several times and then dried in air at 70 °C overnight; they were readily redispersed in various polar organic solvents.

Powder X-ray diffraction (XRD) patterns of the dried powders were recorded on a Philips PW 1140/90 diffractometer with Cu Kα radiation at a scan rate of 2 min^{-1} and a step size of 0.02°. Field-emission scanning electron microscopy (FE-SEM) images were obtained with a JEOL JSM-6300F microscope operated at 10.0 kV. TEM and high-resolution TEM (HRTEM) characterizations were performed with a JEOL 3000F microscope (Japan) operated at 300 kV. Nitrogen adsorption–desorption experiments were performed at 77 K using a Micromeritics ASAP 2020MC instrument. The samples were degassed at 350 °C for 6 h prior to examination. The surface areas were estimated according to the Brunauer–Emmett–Teller (BET) method, and the pore-size distributions were calculated based on the Barrett–Joyner–Halenda (BJH) method. Fourier transform infrared spectroscopy (FT-IR) data was collected using a Perkin–Elmer Spectrum 100 FT-IR spectrometer. Room temperature fluorescence spectra of 1.0 wt% $LaPO_4$:Ce,Tb nanocrystals dispersed in ethanol were recorded on a Perkin–Elmer LS-50B luminescence spectrophotometer equipped with a 150 W Xe arc lamp at a fixed bandpass of 0.2 nm with the same instrument parameters (2.5 nm for excitation slit, 2.5 nm for emission slit, and 700 V for PMT voltage).

Acknowledgements

The authors are grateful for financial support from NSFC (20671087) and the National Basic Research Program of China (2007CB925101), and the Australian Research Council (ARC).

References

1 X. G. Peng, L. Manna, W. D. Yang, J. Wickham, E. Scher, A. Kadavanich and A. P. Alivisatos, *Nature*, 2000, **404**, 59–61.
2 R. C. Jin, Y. W. Cao, C. A. Mirkin, K. L. Kelly, G. C. Schatz and J. G. Zheng, *Science*, 2001, **294**, 1901–1903.
3 C. Burda, X. B. Chen, R. Narayanan and M. A. El-Sayed, *Chem. Rev.*, 2005, **105**, 1025–1102.
4 L. S. Li and A. P. Alivisatos, *Adv. Mater.*, 2003, **15**, 408–411.

5 Y. W. Jun, J. W. Seo, S. J. Oh and J. Cheon, *Coord. Chem. Rev.*, 2005, **249**, 1766–1775.
6 B. Liu and H. C. Zeng, *J. Am. Chem. Soc.*, 2004, **126**, 8124–8125.
7 D. S. Wang, T. Xie, Q. Peng and Y. D. Li, *J. Am. Chem. Soc.*, 2008, **130**, 4016–4022.
8 J. Yang, C. X. Li, X. M. Zhang, Z. W. Quan, C. M. Zhang, H. Y. Li and J. Lin, *Chem.–Eur. J.*, 2008, **14**, 4336–4345.
9 C. B. Murray, C. R. Kagan and M. G. Bawendi, *Annu. Rev. Mater. Sci.*, 2000, **30**, 545–610.
10 M. P. Pileni, *J. Phys. Chem. B*, 2001, **105**, 3358–3371.
11 H. Colfen and S. Mann, *Angew. Chem., Int. Ed.*, 2003, **42**, 2350–2365.
12 Z. Y. Huo, C. Chen and Y. D. Li, *Chem. Commun.*, 2006, 3522–3524.
13 O. Lehmann, K. Kompe and M. Haase, *J. Am. Chem. Soc.*, 2004, **126**, 14935–14942.
14 H. Onoda, H. Nariai, A. Moriwaki, H. Maki and I. Motooka, *J. Mater. Chem.*, 2002, **12**, 1754–1760.
15 L. Y. Wang, R. X. Yan, Z. Y. Hao, L. Wang, J. H. Zeng, H. Bao, X. Wang, Q. Peng and Y. D. Li, *Angew. Chem., Int. Ed.*, 2005, **44**, 6054–6057.
16 L. H. Qu and X. G. Peng, *J. Am. Chem. Soc.*, 2002, **124**, 2049–2055.
17 C. Xue and C. A. Mirkin, *Angew. Chem., Int. Ed.*, 2007, **46**, 2036–2038.
18 K. W. Kramer, D. Biner, G. Frei, H. U. Gudel, M. P. Hehlen and S. R. Luthi, *Chem. Mater.*, 2004, **16**, 1244–1251.
19 K. Hickmann, K. Kömpe, A. Hepp and M. Haase, *Small*, 2008, **4**, 2136–2139.
20 M. J. Fisher, W. Z. Wang, P. K. Dorhout and E. R. Fisher, *J. Phys. Chem. C*, 2008, **112**, 1901–1907.
21 Z. X. Fu and W. B. Bu, *Solid State Sci.*, 2008, **10**, 1062–1067.
22 P. Ghosh and A. Patra, *J. Nanosci. Nanotechnol.*, 2008, **8**, 3458–3464.
23 Y. P. Fang, A. W. Xu, R. Q. Song, H. X. Zhang, L. P. You, J. C. Yu and H. Q. Liu, *J. Am. Chem. Soc.*, 2003, **125**, 16025–16034.
24 R. X. Yan, X. M. Sun, X. Wang, Q. Peng and Y. D. Li, *Chem.–Eur. J.*, 2005, **11**, 2183–2195.
25 H. X. Mai, Y. W. Zhang, L. D. Sun and C. H. Yan, *Chem. Mater.*, 2007, **19**, 4514–4522.
26 K. Rajesh, P. Mukundan, P. K. Pillai, V. R. Nair and K. G. K. Warrier, *Chem. Mater.*, 2004, **16**, 2700–2705.
27 L. Li, W. G. Jiang, H. H. Pan, X. R. Xu, Y. X. Tang, J. Z. Ming, Z. D. Xu and R. K. Tang, *J. Phys. Chem. C*, 2007, **111**, 4111–4115.
28 S. Nishihama, T. Hirai and I. Komasawa, *J. Mater. Chem.*, 2002, **12**, 1053–1057.
29 G. Buehler and C. Feldmann, *Angew. Chem., Int. Ed.*, 2006, **45**, 4864–4867.
30 M. Yu, J. Lin, J. Fu, H. J. Zhang and Y. C. Han, *J. Mater. Chem.*, 2003, **13**, 1413–1419.

